Table 4. Average SUVR between 20 and 40 min after injection

	SUVR					Cohen's d	
	aged normal	MCI-NC	MCI-C	AD1	AD2	MCI-NC and MCI-C	aged normal and all AD
Frontal	0.98 ± 0.05	0.98 ± 0.06	1.11 ± 0.10*, #	1.08 ± 0.08*	1.06 ± 0.05	1.62	1.69
Temporal	1.02 ± 0.04	1.06 ± 0.07	1.18 ± 0.07*, #	1.18 ± 0.07*, #	1.18 ± 0.06*, #	1.7	2.93
Parietal	1.06 ± 0.04	1.08 ± 0.05	1.17 ± 0.05*	1.18 ± 0.06*, #	1.19 ± 0.09*	1.76	2.25
Occipital	1.05 ± 0.04	1.09 ± 0.06	1.11 ± 0.06	1.13 ± 0.07*	1.13 ± 0.05*	0.37	1.51
Posterior cingulate	1.11 ± 0.07	1.12 ± 0.07	1.19 ± 0.10	1.20 ± 0.09	1.22 ± 0.05*	0.85	1.51

Values denote means ± SD. * $p < 0.05$ versus aged normal group; # $p < 0.05$ versus MCI-NC group.

tal cortex. In the temporal cortex, the number of positively stained Aβ plaques showed a significantly positive correlation with the number of dense- and diffuse-type plaques. However, in the frontal cortex, the number of positively stained Aβ plaques showed a significant correlation with only the number of dense-type plaques and not with the number of diffuse-type plaques (fig. 6).

Discussion

The identification of patients with a high risk of developing AD in the MCI stage is of great clinical value. However, it is difficult to predict the conversion from MCI to AD from a clinical and neuropsychological perspective. In comparison with MRI and CT, PET is relatively expensive and not accessible. Consequently, PET is not routinely used in the diagnosis of AD. However, PET imaging provides useful diagnostic information for predicting conversion from MCI to AD when MRI fails to provide sufficient information [15]. A recent Pittsburgh compound B (PiB) PET study demonstrated that in vivo detection of amyloid deposition provides useful prognostic information in MCI [19]. The present study using BF-227 PET showed similar predictive performance to previous PiB PET results although the signal-to-background ratio increase for BF-227 in patients with AD over controls was considerably lower than that for PiB. The lower signal-to-background ratio of BF-227 would be due to the lower detection sensitivity of BF-227 than that of PiB for diffuse plaques. However, BF-227 PET may have a better predictive value for progression from MCI to AD than PiB PET because the deposition of diffuse plaque is observed even during the normal aging process. A head-to-head comparison of BF-227 PET with PiB PET will clarify which tracer has more predictive power for conversion of MCI to AD.

Voxel-based analysis of PET images allows an objective and sensitive identification of regional change in uptake of the tracer. BF-227 is a PET tracer that binds to amyloid plaques in the brain [10]. Although BF-227 binds well to amyloid fibrils in vitro, the signal-to-background ratio for [^{11}C]BF-227 PET images was relatively lower than that for PiB PET, possibly due to the lower binding affinity of BF-227 to Aβ fibrils compared to PiB. This drawback can be overcome by voxel-based statistical comparison with a normal control database. In fact, the abnormal distribution of [^{11}C]BF-227 in MCI-C was more clearly demonstrated by Z-score mapping analysis than by unprocessed SUVR images. In addition, a portion of MCI-NC showed a high Z-score in the posterior neocortical areas, which may reflect early Aβ pathology in the brain. The pathological significance of these abnormalities will be elucidated after having followed up these patients.

A commonly observed feature in the Z-score maps of MCI-C and patients with AD was the change in bilateral temporal and temporooccipital cortices, which was also detected by between-group comparison with the aged

Fig. 2. a Voxel-by-voxel Z-score analysis of [^{11}C]BF-227 PET images for aged normal subjects (left) and patients with AD (right) with the mean and SD of PET images of 15 normal controls. The Z-score maps were displayed by the surface projection of the spatially normalized MR image. **b** Voxel-by-voxel Z-score analysis by comparison of [^{11}C]BF-227 PET images for MCI-NC (left) and MCI-C (right) with the mean and SD of PET images of 15 normal controls. The Z-score maps were displayed by the surface projection of the spatially normalized MR image.

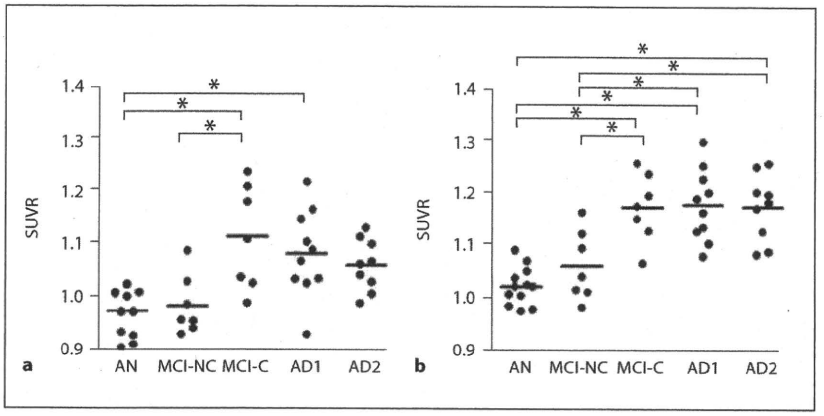

Fig. 3. Regional BF-227 SUVR in the frontal (**a**) and temporal (**b**) cortices. Horizontal bar: average SUVR in each group. * $p <$ 0.05.

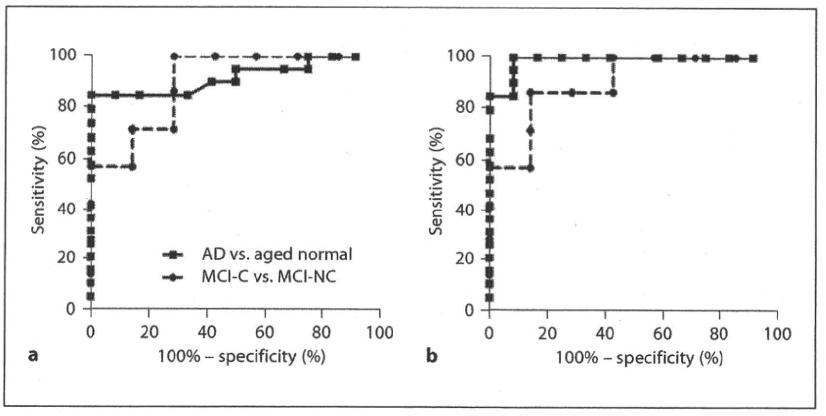

Fig. 4. ROC curves of regional BF-227 SUVR in the frontal (**a**) and temporal (**b**) cortices for differentiation between patients with AD and aged normal controls (solid line) and between MCI-C and MCI-NC (dashed line).

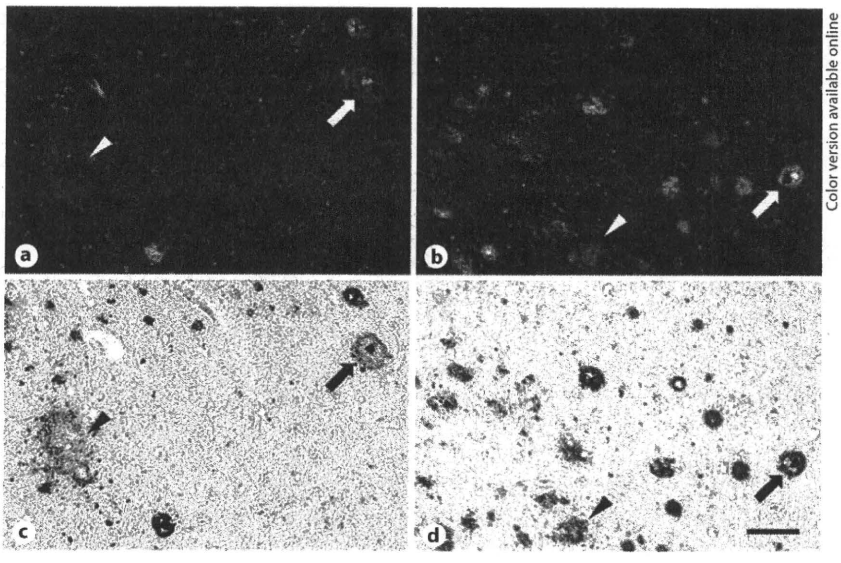

Fig. 5. Neuropathologic staining of AD frontal (**a**, **c**) and temporal (**b**, **d**) brain sections by BF-227. Cored plaques (arrows) are clearly stained with BF-227 (**a**, **b**). Cored-plaque staining with BF-227 correlates well with Aβ immunostaining in adjacent sections (**c**, **d**). Diffuse plaques (arrowheads) are faintly stained with BF-227 in the frontal brain section (**a**), but moderately stained in the temporal brain section (**b**). Scale bar = 100 μm.

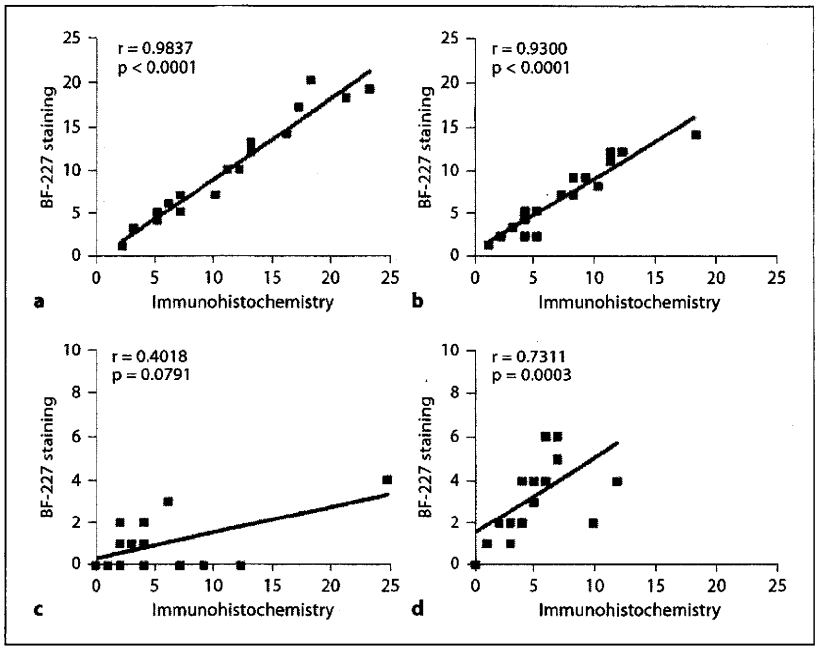

Fig. 6. Correlations between the numbers per unit area of amyloid plaques stained with Aβ-specific antibody and BF-227. The density of dense-type plaques showed a significant correlation with positive staining with BF-227 both in the frontal (**a**) and temporal (**b**) brain sections. However, the density of diffuse-type plaques was not correlated with BF-227 staining in the frontal cortex (**c**), and weakly correlated with BF-227 staining in the temporal cortex (**d**).

normal controls using the SPM software. The preferential [^{11}C]BF-227 retention in the posterior neocortical region corresponded with an area containing a high density of neuritic plaques [20]. This finding was confirmed by our analysis using postmortem AD brain samples. From these findings, the amount of dense plaque deposits in the posterior neocortical region, which could be measured by [^{11}C]BF-227 PET, is a reliable index of prognosis in patients with MCI. Interestingly, the Z-score mapping of BF-227 PET images further elucidated individual variation in the regional distribution of amyloid plaque deposition in patients with AD. There is great interest in determining the relationship between this heterogeneity and the clinical phenotype of patients with AD, which should be investigated in the future with data from a larger population. About 2/3 of patients with AD showed elevated BF-227 uptake in both anterior and posterior association areas, and the remaining 1/3 showed posterior-oriented BF-227 uptake. However, none of the patients with AD showed frontal-oriented BF-227 uptake. Although our analysis has been cross-sectional, these findings suggest that neuritic plaque deposition in AD starts at the posterior association areas and then spreads to other brain regions during AD progression.

The relatively lower [^{11}C]BF-227 retention in the frontal cortex of patients in the AD group may be a chance finding due to the small sample size. However, previous analysis of postmortem AD brain samples indicated that a majority of neocortical plaques start as fibrillar Aβ deposits and, in the late stages of AD, shift to nonfibrillar plaques [21]. Therefore, the relatively lower [^{11}C]BF-227 uptake in the AD group may be due to the transformation of fibrillar Aβ deposits to nonfibrillar Aβ deposits during AD progression. A longitudinal evaluation of [^{11}C]BF-227 uptake is necessary to examine whether the neocortical Aβ deposits reflected by BF-227 uptake change during the course of AD progression. In addition, the quantitative analysis of BF-227 binding to amyloid plaques should be performed in the future to eliminate the influence of regional cerebral hypoperfusion.

The definitive diagnosis of AD depends on postmortem examination because histological analysis of tissue samples is the only method for assessing AD pathology with certainty [7, 22]. Senile plaques were classified on the basis of the morphology of histopathological staining: diffuse plaques, primitive plaques, classical plaques and compacted plaques [23]. The diffuse plaques were abundant in healthy controls, whereas mature plaques such as primitive, classical and compact ones were typical in patients with AD. In our study, strong correlations between the number of mature plaques and BF-227 binding in the frontal and temporal cortices were observed. Further-

more, the temporal cortex exhibited a significant correlation between the number of diffuse-type plaques and BF-227 binding. However, the frontal cortex showed no such correlation. Generally, primitive, classical and compact plaques contain more amyloid fibrils than diffuse plaques. A previous electron microscopic examination has suggested that diffuse plaques in the frontal cortex contain a small amount of amyloid fibrils and do not easily transform to primitive plaques, while those in the temporal cortex contain more amyloid fibrils and tend to transform to primitive plaques [24]. Therefore, the binding ability of BF-227 to different types of diffuse plaques in the frontal and temporal cortices partly explains why BF-227 tends to accumulate in the temporal cortex of the AD brain. In addition, the density of dense-type plaques in the temporal cortex was higher than that in the frontal cortex in our analysis. This finding is in accordance with another comprehensive neuropathological examination that showed a higher density of amyloid plaques in the temporal cortex than in the frontal cortex [20, 25]. Thus, the lower density of primitive plaques in the frontal cortex may explain the relatively lower BF-227 uptake in the frontal cortex. Further analyses using more AD brain samples and radiolabeled BF-227 are required in the future because only one brain was examined in this study, and the concentration of BF-227 used to stain the postmortem tissue was not equivalent to the expected in vivo concentrations.

Previous PiB PET studies have shown the greatest tracer uptake in the precuneus and posterior cingulate cortex. However, our PET study demonstrated greater BF-227 uptake in the lateral temporal and parietal cortices of the AD brain samples than in the posterior cingulate cortex. A recent study demonstrated that the number of diffuse plaques in the posterior cingulate gyrus was greater than that in other neocortical areas. However, the number of neuritic plaques in the posterior cingulate cortex was not greater than that in other neocortical areas during AD progression [26]. Therefore, the modest posterior cingulate BF-227 uptake elevation in some patients with AD may be due to the lower binding affinity of BF-227 to diffuse plaques than that of PiB.

There are several limitations of this study. First, the sample size was small, primarily because of the limited follow-up period. Second, no repeat scans were performed to really assess changes in BF-227 uptake over time. Future studies should include longitudinal data from a larger sample. Third, the patients with MCI were older than the aged normal controls. Therefore, the higher neocortical uptake of [^{11}C]BF-227 in patients with MCI could be attributed to the effect of aging. However, no age-related change in BF-227 uptake was observed in the aged normal controls [10]. Furthermore, no significant elevation of [^{11}C]BF-227 uptake was observed in the MCI-NC group compared with that in the aged normal control group. Therefore, the higher [^{11}C]BF-227 uptake in the MCI-C group is not likely due to the effect of aging. We need to further address this issue by controlling for the age of normal controls and patients with MCI.

In summary, [^{11}C]BF-227 PET can detect the early Aβ load in the lateral temporal cortex of patients with MCI and AD. The amount of [^{11}C]BF-227 uptake in the temporal cortex was strongly related to prognosis in patients with MCI. BF-227 would be less subjective to amyloid pathology during the process of aging since this probe is believed to bind selectively to dense Aβ plaques. Thus, [^{11}C]BF-227 PET offers unique information concerning AD pathology that cannot be obtained by other PET tracers, which would be useful for the MCI population since it allows prediction of their risk for progression to AD in the near future.

Acknowledgments

This study was supported by the Health and Labor Sciences Research Grants for Translational Research from the Ministry of Health and the Grant-in-Aid for Scientific Research on Priority Areas - Integrative Brain Research from the Ministry of Education, Culture, Sports, Science, and Technology of Japan (20019006). We appreciate the technical assistance provided by Dr. S. Watanuki, Dr. Y. Ishikawa and M. Kato during the PET studies.

References

1 Glenner GG, Wong CW: Alzheimer's disease: initial report of the purification and characterization of a novel cerebrovascular amyloid protein. Biochem Biophys Res Commun 1984;120:885–890.

2 Masters CL, Multhaup G, Simms G, Pottgiesser J, Martins RN, Beyreuther K: Neuronal origin of a cerebral amyloid: neurofibrillary tangles of Alzheimer's disease contain the same protein as the amyloid of plaque core and blood vessels. EMBO J 1985;4:2757–2763.

3 Masters CL, Simms G, Weinman NA, Multhaup G, McDonald BL, Beyreuther K: Amyloid plaque core protein in Alzheimer disease and Down syndrome. Proc Natl Acad Sci USA 1985;82:4245–4249.

4 Hardy J, Selkoe DJ: The amyloid hypothesis of Alzheimer's disease: progress and problems on the road to therapeutics. Science 2002;297:353–356.

5 Petersen RC, Smith GE, Waring SC, Ivnik RJ, Tangalos EG, Kokmen E: Mild cognitive impairment: clinical characterization and outcome. Arch Neurol 1999;56:303–308.
6 Petersen RC: Mild cognitive impairment as a diagnostic entity. J Intern Med 2004;256: 183–194.
7 Ikonomovic MD, Klunk WE, Eric E, Abrahamson EE, Mathis CA, Price JC, Tsopelas ND, Lopresti BJ, Ziolko S, Bi WZ, Paljug WR, Debnath ML, Hope CE, Barbara A, Isanski BA, Hamilton RL, DeKosky ST: Post-mortem correlates of in vivo PiB-PET amyloid imaging in a typical case of Alzheimer's disease. Brain 2008;131:1630–1645.
8 Furumoto S, Okamura N, Iwata R, Yanai K, Arai H, Kudo Y: Recent advances in the development of amyloid imaging agents. Curr Top Med Chem 2007;7:1773–1789.
9 Klunk WE, Engler H, Nordberg A, Wang Y, Blomqvist G, Holt DP, Bergström M, Savitcheva I, Huang GF, Estrada S, Ausén B, Debnath ML, Barletta J, Price JC, Sandell J, Lopresti BJ, Wall A, Koivisto P, Antoni G, Mathis CA, Långström B: Imaging brain amyloid in Alzheimer's disease with Pittsburgh Compound-B. Ann Neurol 2004;55:306–319.
10 Kudo Y, Okamura N, Furumoto S, Tashiro M, Furukawa K, Maruyama M, Itoh M, Iwata R, Yanai K, Arai H: 2-(2-[2-dimethylaminothiazol-5-yl]ethenyl)-6-(2-[fluoro]ethoxy)benzoxazole: a novel PET agent for in vivo detection of dense amyloid plaques in Alzheimer's disease patients. J Nucl Med 2007;48:553–561.
11 Furukawa K, Okamura N, Tashiro M, Waragai M, Furumoto S, Iwata R, Yanai K, Kudo Y, Arai H: Amyloid PET in mild cognitive impairment and Alzheimer's disease with BF-227: comparison to FDG-PET. J Neurol 2010;257:721–727.
12 Verhoeff NP, Wilson AA, Takeshita S, Trop L, Hussey D, Singh K, Kung HF, Kung MP, Houle S: In vivo imaging of Alzheimer disease β-amyloid with [^{11}C]SB-13 PET. Am J Geriatr Psychiatry 2004;12:584–595.
13 Okamura N, Suemoto T, Shimadzu H, Suzuki M, Shiomitsu T, Akatsu H, Yamamoto T, Staufenbiel M, Yanai K, Arai H, Sasaki H, Kudo Y, Sawada T: Styrylbenzoxazole derivatives for in vivo imaging of amyloid plaques in the brain. J Neurosci 2004;24: 2535–2541.
14 Okamura N, Furumoto S, Funaki Y, Suemoto T, Kato M, Ishikawa Y, Ito S, Akatsu H, Yamamoto T, Sawada T, Arai H, Kudo Y, Yanai K: Binding and safety profile of novel benzoxazole derivative for in vivo imaging of amyloid deposits in Alzheimer's disease. Geriatr Gerontol Int 2007;7:393–400.
15 Waragai M, Okamura N, Furukawa K, Tashiro M, Furumoto S, Funaki Y, Kato M, Iwata R, Yanai K, Kudo Y, Arai H: Comparison study of amyloid PET and voxel-based morphometry analysis in mild cognitive impairment and Alzheimer's disease. J Neurol Sci 2009;285:100–108.
16 McKhann G, Drachman D, Folstein M, Katzman R, Price D, Stadlan EM: Clinical diagnosis of Alzheimer's disease: report of the NINCDS-ADRDA Work Group under the auspices of Department of Health and Human Services Task Force on Alzheimer's Disease. Neurology 1984;34:939–944.
17 Friston KJ, Holmes AP, Worsley KJ, Poline JP, Frith CD, Frackowiack RSJ: Statistical parametric maps in functional imaging: a general linear approach. Hum Brain Mapp 1995;2:189–210.
18 Matsuda H, Mizumura S, Nagao T, Ota T, Iizuka T, Nemoto K, Takemura N, Arai H, Homma A: Automated discrimination between very early Alzheimer disease and controls using an easy Z-score imaging system for multicenter brain perfusion single-photon emission tomography. AJNR Am J Neuroradiol 2007;28:731–736.
19 Okello A, Koivunen J, Edison P, Archer HA, Turkheimer FE, Någren K, Bullock R, Walker Z, Kennedy A, Fox NC, Rossor MN, Rinne JO, Brooks DJ: Conversion of amyloid positive and negative MCI to AD over 3 years: an ^{11}C-PiB PET study. Neurology 2009;73:754–760.
20 Arnold SE, Hyman BT, Flory J, Damasio AR, van Hoesen GW: The topographical and neuroanatomical distribution of neurofibrillary tangles and neuritic plaques in the cerebral cortex of patients with Alzheimer's disease. Cereb Cortex 1991;1:103–116.
21 Wegiel J, Bobinski M, Tarnawski M, Dziewiatkowski J, Popovitch E, Bobinski M, Lach B, Reisberg B, Miller D, de Santi S, de Leon MJ: Shift from fibrillar to nonfibrillar Aβ deposits in the neocortex of subjects with Alzheimer disease. J Alzheimers Dis 2001;3:49–57.
22 Braak H, Braak E: Neuropathological staging of Alzheimer-related changes. Acta Neuropathol 1991;82:239–259.
23 Dickson DW: The pathogenesis of senile plaques. J Neuropathol Exp Neurol 1997;56: 321–339.
24 Yamaguchi H, Nakazato Y, Shoji M, Takatama M, Hirai S: Ultrastructure of diffuse plaques in senile dementia of the Alzheimer type: comparison with primitive plaques. Acta Neuropathol 1991;82:13–20.
25 Cupidi C, Capobianco R, Goffredo D, Marcon G, Ghetti B, Bugiani O, Tagliavini F, Giaccone G: Neocortical variation of Aβ load in fully expressed, pure Alzheimer's disease. J Alzheimers Dis 2010;19:57–68.
26 Nelson PT, Abner EL, Scheff SW, Schmitt FA, Kryscio RJ, Jicha GA, Smith CD, Patel E, Markesbery WR: Alzheimer's-type neuropathology in the precuneus is not increased relative to other areas of neocortex across a range of cognitive impairment. Neurosci Lett 2009;450:336–339.

J Neuropathol Exp Neurol
Copyright © 2010 by the American Association of Neuropathologists, Inc.

Vol. 69, No. 7
July 2010
pp. 00–00

ORIGINAL ARTICLE

Neuropathological Asymmetry in Argyrophilic Grain Disease

Tadashi Adachi, MD, Yuko Saito, MD, PhD, Hiroyuki Hatsuta, MD, Sayaka Funabe, MD, Aya M. Tokumaru, MD, PhD, Kenji Ishii, MD, Tomio Arai, MD, PhD, Motoji Sawabe, MD, PhD, Kazutomi Kanemaru, MD, PhD, Akinori Miyashita, PhD, Ryozo Kuwano, MD, PhD, Kenji Nakashima, MD, PhD, and Shigeo Murayama, MD, PhD

Abstract

The presence of argyrophilic grains in the neuropil is associated with a form of dementia. We investigated morphological asymmetry in 653 consecutive autopsy patients from a general geriatric hospital (age [mean ± SD] = 81.1 ± 8.9 years), focusing on those from patients with advanced argyrophilic grain disease. Paraffin sections of the bilateral posterior hippocampi were immunostained with anti–phosphorylated tau and anti–4-repeat tau antibodies and by the Gallyas-Braak method. In a side-to-side comparison, asymmetry was defined when either the extent or the density of argyrophilic grains was different. Of the 653 subjects, 65 (10%) had Stage 3 argyrophilic grain disease, and 59 (90.8%) showed histopathological asymmetry. Antemortem computed tomographic images (n = 24), magnetic resonance imaging scans (n = 8), and combined computed tomographic and magnetic resonance images (n = 15) were available; images from 20 of the 47 subjects showed asymmetry that correlated with the histopathological asymmetry. Cerebral cortical asymmetry consistent with the histopathology was also visible in *N*-isopropyl-^{123}I-*p*-iodoamphetamine single photon emission computed tomographic images from 6 patients and ^{18}F-labeled fluorodeoxyglucose positron emission tomographic images from 2 patients. Thus, asymmetric involvement of the medial temporal lobe in patients with advanced argyrophilic grain disease may represent a diagnostic feature and contribute to distinguishing dementia with grains from Alzheimer disease.

Key Words: Alzheimer disease, Argyrophilic grain, Asymmetry, Dementia, MRI, Neuroimaging, tau Protein.

From the Department of Neuropathology (TA, YS, HH, SF, SM) and Positron Medical Center (KI), Tokyo Metropolitan Institute of Gerontology; Departments of Pathology (HH, TA, MS), Radiology (AMT), and Neurology (KK), Tokyo Metropolitan General Hospital, Tokyo; Department of Molecular Genetics (AM, RK), Center for Bioresources, Brain Research Institute, Niigata University, Niigata; and Division of Neurology (TA, KN), Department of Brain and Neurosciences, Faculty of Medicine, Tottori University, Tottori, Japan.

Send correspondence and reprint requests to: Shigeo Murayama, MD, PhD, Department of Neuropathology, Tokyo Metropolitan Institute of Gerontology, 35-2 Sakaecho, Itabashi-ku, Tokyo 173-0015, Japan; E-mail: smurayam@tmig.or.jp

This study was supported by an Aid for Scientific Research on Priority Areas—Advanced Brain Science Project—from the Ministry of Education, Culture, Sports, Science, and Technology of Japan (S.M.).

A part of this study was presented at the 85th Annual Meeting of the American Association of Neuropathologists, June 2009, San Antonio, TX.

INTRODUCTION

Argyrophilic grains (AGs), first reported by Braak and Braak in 1987, consist of punctate or filiform structures in the neuropil that can be visualized by Gallyas-Braak silver staining (1). Dementia with grains (DG), as defined by Braak and Braak (1, 2) and Jellinger (3), is a form of senile dementia in which AGs are the sole morphological substrate that can explain the dementia. Argyrophilic grains accompanied neuronal cytoplasmic tau immunoreactivity (IR; pretangle), tau-positive astrocytes (bush-like astrocytes), oligodendroglial coiled bodies, and ballooned neurons (4). Ultrastructurally, AGs consist of a straight filament 9 to 18 nm in diameter and bundles of smooth tubules 25 nm in diameter and are thought to be localized in dendritic spines (5).

Argyrophilic grains consist of a 4-repeat isoform of tau protein (6–8), and antibodies directed against the 4-repeat tau are the most sensitive markers for the grains (9). We have reported that the severe involvement of the ambient gyrus is a unique pathological feature of DG (10, 11) and proposed a staging paradigm for AGs that starts with the involvement of the ambient gyrus and amygdala (Stage 1: ambient stage), then expands to include the posterior parahippocampal gyrus and medial anterior temporal pole (Stage 2: medial temporal stage), and finally spreads to the basal forebrain and anterior cingulate gyrus (Stage 3: frontal lobe stage) (12). Our staging scheme was recently supported by Ferrer et al (13) and Santpere and Ferrer (14).

In the process of screening unselected brains obtained from consecutive autopsy patients at our institute, we have frequently encountered asymmetry in the density or in the extent in AGs in cases that carry the abnormal structures. Because dementia in DG is usually associated with Stage 3 AG (12), we focused our investigation on this advanced stage of grain disease and characterized AG asymmetry in a systematic manner and correlated the findings with available neuroimaging. Our data on the asymmetry in the density and extent of grains, combined with the preferential atrophy of the ambient gyrus, may contribute to enhanced neuroimaging diagnosis of DG.

MATERIALS AND METHODS

Tissue Source

Brains and spinal cords were obtained from 653 consecutive autopsies at Tokyo Metropolitan Geriatric Hospital

and Institute of Gerontology between June 2001 and December 2007. The ages of the subjects at death ranged from 52 to 104 years (mean ± SD = 81.1 ± 8.9 years), and the male-to-female ratio was 361:292.

Neuropathology

The brains and spinal cords were examined as previously reported (15). Briefly, one hemisphere was preserved for biochemical and molecular studies, and the other was prepared for morphological studies. At autopsy, 1 cerebral hemisphere was sliced in the coronal plane at 7-mm intervals. The brainstem was sectioned in the axial planes in 5-mm-thick slices, and the cerebellum was sectioned in sagittal planes in 5-mm-thick slices. The following anatomical areas were sampled: frontal, temporal, and occipital poles, parietal lobe including intraparietal sulcus, anterior amygdala, posterior hippocampus, dentate nucleus, and midbrain. The samples were fixed in 4% paraformaldehyde for 48 hours and embedded in paraffin. The other half of the brain was fixed in 20% buffered formalin for 7 to 13 days and sliced in the same manner as that performed in the contralateral hemisphere, and the representative areas were embedded in paraffin. We adjusted these fixation times for the frozen half and fixed half sides to compensate both for optimal fixation and for comparative morphological observations in AT8 immunohistochemistry (IHC) at the start of our brain bank in 1999. Six-micrometer-thick serial sections were stained with hematoxylin and eosin and by the Klüver-Barrera method. Selected sections were further examined with modified methenamine (16) and Gallyas-Braak (17) staining for senile changes, Congo red for amyloid deposition, and elastica Masson trichrome stain for vascular changes.

Immunohistochemistry

Selected sections were immunostained using an autostainer (Ventana 20NX; Ventana, Tucson, AZ), as previously reported (12). The antibodies included anti–phosphorylated tau (ptau; AT8, monoclonal; Innogenetics, Temse, Belgium), anti–4-repeat tau (RD4, monoclonal; Upstate, Lake Placid, NY), anti–phosphorylated α-synuclein (psyn; monoclonal, psyn no. 64 [18]), anti–β-amyloid 11–28 (12B2, monoclonal; IBL, Maebashi, Japan), antiubiquitin (polyclonal; DAKO, Glostrup, Denmark), and anti–phosphorylated TAR DNA-binding protein of 43 kd (TDP43; PSer409/410; monoclonal, a gift from Dr M. Hasegawa, Tokyo Institute of Psychiatry), as previously reported (18).

Apolipoprotein E Genotyping

Genomic DNA was extracted from freshly frozen kidneys of 577 patients (obtained from June 2001 to November 2006). DNA concentrations were measured with a spectrophotometer (U2000; Hitachi, Tokyo, Japan) adjusted to 100 μg/mL. Tissues from all but 7 patients (6 patients with Creutzfeldt-Jakob disease and 1 patient with global hypoxic ischemic changes) were genetically examined. After polymerase chain reaction amplification (19), apolipoprotein E (APOE) genotyping was conducted with the restriction enzyme *Hha*I, as described by Hixson and Vernier (20). From the freshly frozen brains of 69 patients (obtained from December 2006 to December 2007), APOE genotyping of all samples was performed by direct cycle sequencing with an ABI 3100 sequencer and a BigDye Terminator v3.1 kit (Applied Biosystems) using the following primers: C19APOE001-F (sense 5′-GCCTACAAATCGGAACTGGA-3′) and C19APOE001-R (antisense 5′- ACCTGCTCCTTCACCTCGT-3′) (21). AQ1

Clinical Data

Clinical information was retrospectively obtained from the medical charts as well as from interviews with patients' attending physicians and caregivers. The Mini-Mental State Examination (22) or Hasegawa Dementia Screening scale (or its revised version) (23) and the Instrumental Activities of Daily Living scale (24) were used to evaluate cognitive function. The Clinical Dementia Rating (CDR) scale (25) was retrospectively determined by 2 independent board-certified neurologists.

Neuropathological Diagnosis

Neurofibrillary tangles (NFTs) were classified into 7 stages (from 0 to 6), and senile plaques were classified into 4 stages (0 and from A to C) according to the criteria of Braak and Braak (26). Argyrophilic grains were classified into our 4 stages (from 0 to 3) as previously reported (12). The neuropathological diagnosis of Alzheimer disease (AD) was based on our definition (27), which proposes a modification of the National Institute on Aging–Reagan criteria. The diagnosis of DG and "neurofibrillary tangle–predominant form of senile dementia (NFTD)" was based on the definition of Jellinger (3) and Jellinger and Bancher (28). The diagnosis of dementia with Lewy bodies (DLB) was based on the revised consensus guidelines (29). The diagnosis of progressive supranuclear palsy (PSP) was based on the National Institute of Neurological Disorders and Stroke criteria (30). The diagnosis of corticobasal degeneration (CBD) was based on the National Institutes of Health criteria (31). The diagnosis of vascular dementia was based on the criteria of the National Institute of Neurological Disorders and Stroke Association Internationale pour la Recherche et l'Enseignement en Neurosciences (32).

Case Selection and Subclassification of Cases With AG Stage 3

All of the patients who were categorized into AG Stage 3 were subclassified into the following 4 forms: the "pure form" represented AGs without any vascular or neurodegenerative changes that could explain cognitive decline, fulfilling Braak NFT Stage 2 or lower and the brain bank for Aging Research Lewy Stage 1 or lower (33); the "NFT form" contained NFTs with the Braak NFT Stage 3 or higher and senile plaque Stage A or lower (26); the "mixed form" is complicated by vascular pathology or metabolic disorders that could explain the cognitive decline; and the "combined form" containing neurodegenerative pathology other than AG itself fulfilled the diagnostic criteria of certain demential disorders.

Evaluation of AGs and Related Structures

Argyrophilic grains were defined as round- or comma-shaped structures with a diameter greater than 1 μm in the neuropil. Bilateral sections of the anterior amygdala and posterior hippocampus at the level of the lateral geniculate body were stained with the Gallyas-Braak silver method and by IHC with AT8 and RD4. Gallyas-Braak silver staining was more sensitive for identifying AGs in 20% buffered

Fig 1 4/C

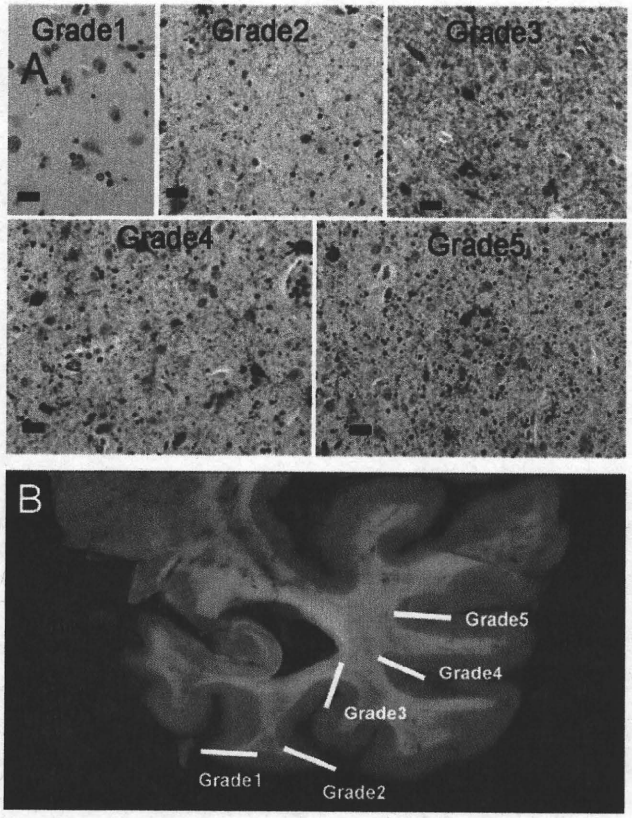

FIGURE 1. Extent and density grading of argyrophilic grains (AGs). **(A)** Density grades were obtained by counting AGs visualized with AT8 immunostain in high-power fields (HPFs; original magnification: 400×), in the entorhinal cortex at the level of the posterior hippocampus. Argyrophilic grains with a diameter greater than 1 μm were counted. Grade 1, 0 to 20/HPF; Grade 2, 20 to 50/HPF; Grade 3, 50 to 100/HPF; Grade 4, 100 to 200/HPF; Grade 5, greater than 200/HPF. Bar = 20 μm. **(B)** Argyrophilic grain extent grades were as follows: Grade 1, localized to the entorhinal cortex (parahippocampal gyrus); Grade 2, spreading to the crown of the fusiform gyrus (T4); Grade 3, to the valley of T4; Grade 4, to the inferior temporal gyrus; and Grade 5, to the middle temporal gyrus.

formalin-fixed sections than in 4% paraformaldehyde-fixed sections. In contrast, RD4 IHC was more sensitive for AGs in paraformaldehyde-fixed sections. AT8 IHC detected AGs to the same extent in both sections, as determined when we started our brain bank. Therefore, we compared the density of AG with AT8 IHC as follows: AGs were counted at a magnification of 400× in the basolateral nucleus of the bilateral amygdala and the entorhinal cortex of the posterior hippocampus and were classified to the following grades: Grade 1, 0 to 20; Grade 2, 20 to 50; Grade 3, 50 to 100; F1 Grade 4, 100 to 200; and Grade 5, more than 200 (Fig. 1A).

To assess the extent of AGs, the following 5 grades were defined for AT8-stained sections of posterior hippocampus (Fig. 1B): Grade 1, localized to the entorhinal cortex (parahippocampal gyrus); Grade 2, spreading to the crown of fusiform gyrus (T4); Grade 3, to the valley of T4; Grade 4, to the inferior temporal gyrus (T3); and Grade 5, to the middle temporal gyrus (T2). Histopathological asymmetry was interpreted as present when there was any difference in the extent or density of grading between the 2 hemispheres.

We also counted the numbers of neuronal cytoplasmic AT8-IR inclusions (pretangles) in the granular layer of the dentate gyrus and classified them semiquantitatively as follows: Grade 1, 0 to 10/section; Grade 2, 10 to 40/section; Grade 3, 40 to 100/section; and Grade 4, more than 100/section. Asymmetry was defined when there was any difference between the right and left side.

Evaluation of Alzheimer-Type NFTs

In addition to Braak NFT stage, the AT8 staging of NFTs by the European Brain Net Consortium (34) was modified and used for this study. AT8 IHC was applied to the bilateral anterior amygdala, posterior hippocampi, and occipital cortex, and AT8 staging of the both sides was compared.

Evaluation of Clinical Images

Clinical images (computed tomography [CT], magnetic resonance imaging [MRI], *N*-isopropyl-^{123}I-*p*-iodoamphetamine single photon emission computed tomography [^{123}I-IMP-SPECT], ^{18}F-labeled fluorodeoxyglucose positron emission tomography [^{18}F-FDG-PET]) from our series were selected retrospectively and evaluated independently and blindly by 2 neurologists and a neuroradiologist (A.M.T.).

Statistical Analysis

Statistical analyses were performed with the χ^2 test or the Fisher exact test for comparisons of categorical data. Correlations between the extent and density grades of AGs in posterior hippocampus were assessed with the Spearman rank correlation coefficient. The Mann-Whitney *U* test was used for comparison of age at death, CDR score, and Braak NFT stage. All statistical analyses were performed using SPSS 15.0J for Windows (SPSS, Inc, Chicago, IL). The threshold for statistical significance was set at $p < 0.05$.

RESULTS

Clinical Data on Cognitive Decline

The CDR could be retrospectively assessed in 590 patients: CDR 0 (n = 214), CDR 0.5 (n = 85), CDR 1 (n = 123), CDR 2 (n = 40), and CDR 3 (n = 128). Thus, 63.7% had CDR 0.5 or higher (mild cognitive impairment or dementia).

TABLE 1. Correlation Between Extent and Density Grades of AGs in the Posterior Hippocampus

		Density Grade				
		1	2	3	4	5
Extent grade	1	10/6	0/1	0/0	0/0	0/0
	2	4/7	4/3	1/0	0/0	0/0
	3	4/2	3/1	3/3	2/2	0/0
	4	2/1	6/9	8/8	3/7	3/0
	5	1/0	0/3	3/5	6/5	2/2

The numbers correspond to right side/left side.
$r = 0.674$, $p < 0.001$.

TABLE 2. Demographic Data and Asymmetry in AGs in 65 Patients With AGs Stage 3

	Histopathological Asymmetry				Asymmetry in Each Grade			Dominant* Side		
	Total	No	Yes	p	Extent	Severity	p	Right	Left	p
No. cases	65	6	59		37	48		23	36	
Male/female	37:28	2:4	35:24	0.39	24:13	27:21	0.56	13:10	22:14	0.79
Age (years), mean ± SD	84.2 ± 7.6	88.5 ± 7.8	83.8 ± 7.4	0.15	83.1 ± 6.9	83.9 ± 7.4	0.57	84.1 ± 6.5	83.6 ± 7.9	0.81
CDR ≥ 0.5, n	56	5	51	0.13	30	46	0.83	19	32	0.94
CDR ≥ 1, n	42	4	38	0.07	22	35	0.66	15	23	0.60
APOE ε4 carriers	9	0	9	0.58	5	8	0.92	4	5	1.00
Braak NFT stage, mean	2.34	3.5	2.2	0.01	1.86	2.31	0.06	2.3	2.17	0.66
Braak SP stage, n										
0–A	44	4	40	0.58	27	32	0.69	17	23	0.51
B–C	21	2	19	0.57	10	16	0.70	6	13	0.32

*Side with greater either extent or density of AGs.
SP, senile plaque.

Neuropathological Diagnosis

The neuropathological diagnoses, excluding AG Stage 3 patients, consisted of AD (n = 71), Parkinson disease/Parkinson disease with dementia/DLB (n = 35), PSP (n = 14), vascular dementia (n = 12), NFTD (n = 12), amyotrophic lateral sclerosis (ALS)/ALS with dementia (n = 12), Creutzfeldt-Jakob disease (n = 6), hippocampal sclerosis (n = 6), CBD (n = 2), multiple-system atrophy (n = 3), Machado-Joseph disease (n = 3), Huntington disease (n = 2), and frontotemporal lobar degeneration with TDP43-IR inclusions (n = 1). Comorbid demential pathologies included AD plus DLB (n = 11), Parkinson disease with dementia plus PSP (n = 4), and AD plus vascular dementia (n = 1). The remaining patients did not fulfill clinical and/or pathological criteria for any single neurodegenerative disease.

Among the 653 subjects, 65 (10%) were classified into Brain Bank for Aging Research AG Stage 3. These 65 patients were further subclassified as pure form (n = 15, 23.1%), NFT form (n = 14, 21.5%), mixed form (n = 22, 33.8%), and combined form (n = 14, 21.5%). The degenerative pathological diagnoses of the combined form included PSP (n = 5), CBD (n = 3), AD (n = 2), DLB (n = 1), AD+DLB (n = 1), PSP + DLB (n = 1), ALS with dementia (n = 1), and ALS (n = 1).

Clinical Features of AG Stage 3 Patients

The ages at death of the 65 patients with AG Stage 3 ranged from 68 to 97 years (84.2 ± 7.6 years). The male-to-female ratio was 37:28. The CDR score could be retrospectively determined for 64 of these patients: CDR 0 (n = 8), CDR 0.5 (n = 14), CDR 1 (n = 17), CDR 2 (n = 5), and CDR 3 (n = 20). Thus, the CDR of 56 (87.5%) of the 64 patients was 0.5 or higher, corresponding to amnestic mild cognitive impairment or dementia. The clinical diagnoses of these patients were either AD or vascular dementia.

Histopathological Asymmetry of AGs and Related Structures

The histopathological asymmetry in the density grades of AG in the anterior amygdala was present in 32 (49.2%) of the 65 patients with AG Stage 3. The asymmetry was commensurate with the asymmetry in the density grades in the posterior hippocampus.

The extent and density grades of AG in the bilateral posterior hippocampus were strongly correlated ($r = 0.674$, $p < 0.001$; Table 1). Histopathological asymmetry was present in 59 (90.8%) of the 65 patients (Table 2). When compared in extent grade or in density grade alone, histopathological

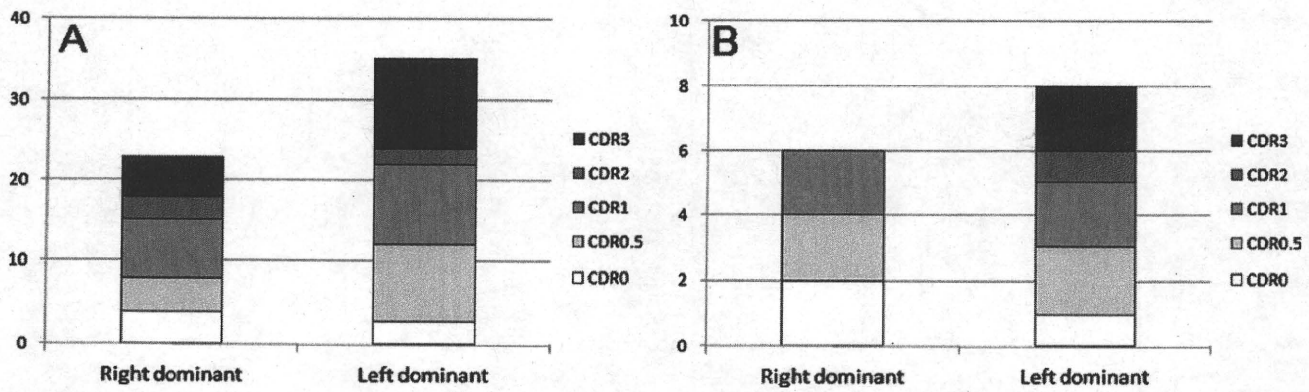

FIGURE 2. Clinical Dementia Rating scales. **(A)** Clinical Dementia Rating scores are not statistically significant among all subjects with argyrophilic grain Stage 3 (p = 0.735). **(B)** Of cases with the "pure form" of argyrophilic grain, only those with more extensive argyrophilic grain on the left side had Clinical Dementia Rating score of 2 or higher. The y axes indicate numbers of cases.

TABLE 3. Correlation of Pathological and Radiological Findings in Patients With AG Stage 3

		Histopathological Asymmetry			
		No	Yes		
	Total		Right-Dominant	Left-Dominant	p
No. cases	65	6	23	36	
Morphological imaging	47 (CT, n = 39; MRI, n = 23)	5	17	25	
No asymmetry	27	5	6	16	
Right-dominant	11	0	11	0	
Left-dominant	9	0	0	9	<0.001
Functional imaging	7 (PET, n = 2; SPECT, n = 6)	0	3	4	
No asymmetry	0	0	0	0	
Right-dominant	3	0	3	0	
Left-dominant	4	0	0	4	<0.001

asymmetry was present in 37 (56.9%) or in 48 (73.8%) of the 65 patients, respectively. The mean age, male-to-female ratio, and mean Braak NFT stage of the 59 patients with asymmetry were 83.8 ± 7.4, 35:24, and 2.2, respectively; for the 6 patients without asymmetry, they were 88.5 ± 7.8, 2:4, and 3.5, respectively. Braak NFT stage was lower in patients with asymmetry than in patients with symmetry. Statistical difference was not shown between 2 sides when only the extent grade or the density grade was compared. There were 36 patients with left-sided predominance of AG and 23 with right-sided predominance. There was no difference in Braak NFT or senile plaque stage between the right-dominant and the left-dominant patients (Table 2). Although the difference of CDRs of all subjects with AG Stage 3 was not statistically significant, all patients classified as having the pure form and whose CDR was 2 or higher had left-sided predominance of AGs (Fig. 2). All 5 patients with AG Stage 3 combined with PSP and the 3 with CBD had histopathological asymmetry in AG that was commensurate with the histopathological asymmetry of PSP and CBD, i.e. histopathological asymmetry was evaluated in PSP patients semiquantitatively with respect to density of AT8-IR tangles and astrocytes in the bilateral sections of the dentate nucleus, red nucleus and frontal cortex, where the grain-related pretangles and bush-like astrocytes were rarely present. Asymmetry of pretangles in the granular cell layer of the dentate gyrus was present in 32 (49.2%) of 65 cases, which was commensurate with the asymmetry of AG.

Histologic and Neuroimaging Correlations

Computed tomographic and/or MRI scans were available in 47 patients for the evaluation of the asymmetry: CT alone (n = 24), MRI alone (n = 8), and both (n = 15). The mean interval between the last CT or MRI and death was 7 ± 15.6 months. There were 20 patients with asymmetry on CT and/or MRI, 9 with left side–dominant atrophy and 11 with right side–dominant atrophy. In each patient where asymmetry was detected, the direction of the asymmetry assessed by neuroimaging matched that of the histopathological asymmetry (Table 3). In the pure form, 6 (75%) of the 8 patients showed asymmetry in morphological imaging. On the other hand, 3 (37.5%) of the 8 patients in the NFT form, 8 (42.1%) of the 19 patients in the mixed form, and 3 (25%) of the 12 patients in the combined form showed asymmetry in morphological imaging, respectively. Among the 47 patients whose morphological imaging was available, 9 were examined more than twice; 8 of those patients (88.9%) had asymmetry in the first images (mean interval from imaging to death = 3 years 5 months ± 22 months) that was commensurate with the asymmetry in the last images. The remaining patient did not show asymmetry either in the first or in the last image. The sensitivity and specificity for detecting underlying histopathological asymmetry were 50% and 100% for CT and 59% and 100% for MRI. The histopathological differences in the density and extent scores were compared with the presence or absence of asymmetry in structural neuroimages; the more severe the histopathological asymmetry, the more often the asymmetry was present in the images (Table 4).

Functional neuroimages were available for the study of asymmetry in 7 patients, 6 of whom underwent ^{123}I-IMP-SPECT and 2 of whom underwent ^{18}F-FDG-PET. All the functional neuroimages showed asymmetry that correlated with histopathological asymmetry (Fig. 3).

Comparison of Asymmetry Between AG Stage 3 and AD

Among 56 of 71 patients with AD and AG lower than Stage 2 and without significant vascular pathology, histopathological asymmetry in NFT was present in 14 patients. Morphological imaging (CT in 39 patients and/or MRI in 21 patients) was available in 41 of the 56 patients (mean interval between the last CT or MRI and death was 10 ± 14.4 months);

TABLE 4. Correlation Between the Difference of Density or Extent Score and Morphological Asymmetry on Imaging in Patients With Histopathological Asymmetry

	Morphological Asymmetry	
	+	−
Score difference between hemispheres		
1	13	22
≥2	7	1

p = 0.01.
+, asymmetry present; −, no asymmetry.

8 (19.5%) of the 41 patients showed radiological asymmetry. Functional imaging (SPECT and/or PET) was available in 7 of 56 patients and in 4 of the 7 patients who had radiological asymmetry. The number of patients with AG Stage 3 and AD, with or without histopathological asymmetry, was 59 versus 6 in AG and 14 versus 42 in AD-type NFT ($p < 0.001$). Asymmetry in morphological imaging was more often present in AG Stage 3 (20/47, 42.6%) than in AD (12/44, 27.3%; $p < 0.05$).

Influence of APOE ε4 on AGs

The APOE genotypes of patients with AG Stage 3 were as follows: 1 patient with ε2/ε2, 3 patients with ε2/ε3, 52 patients with ε3/ε3, 9 patients with ε3/ε4, and none with

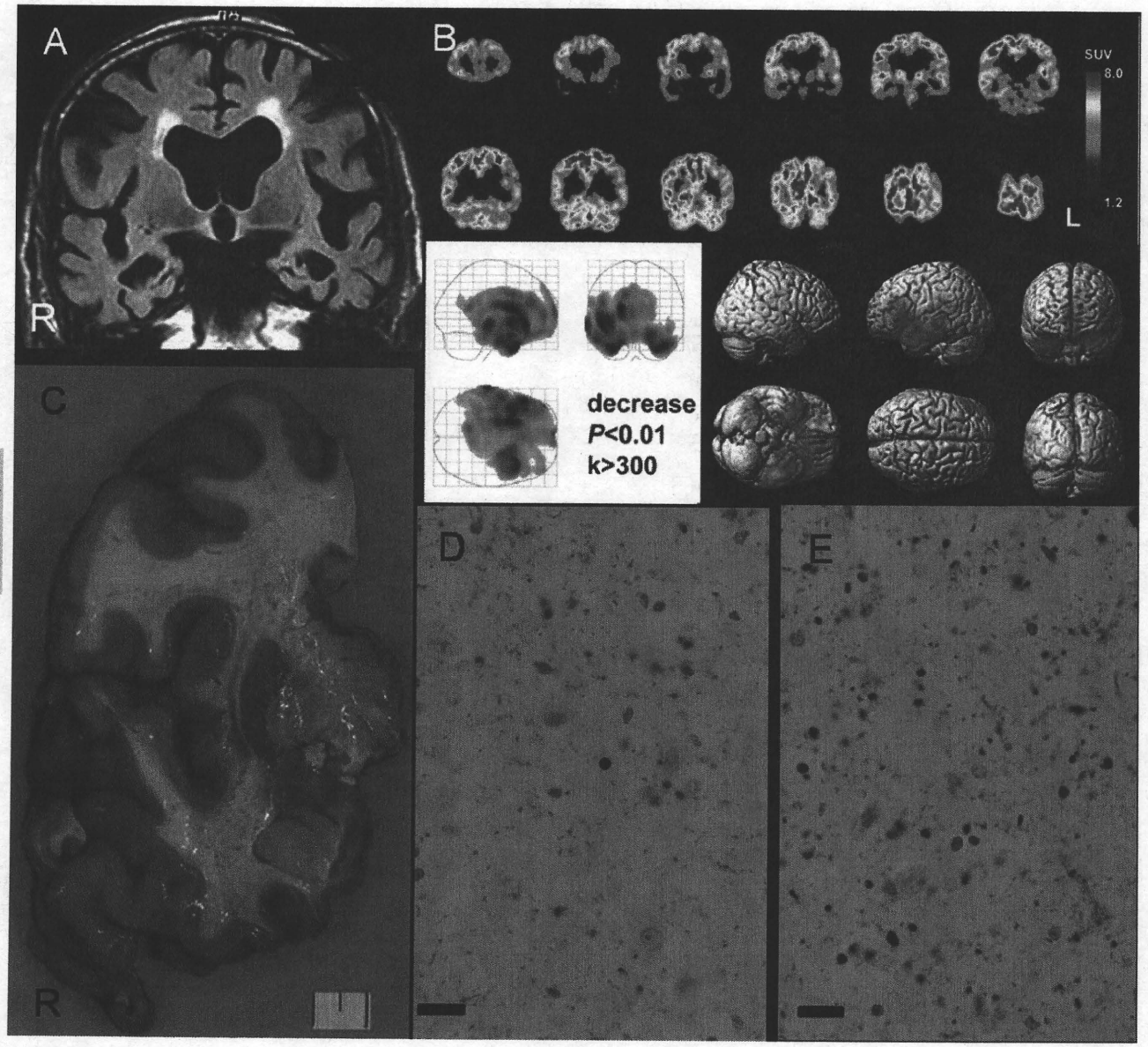

Fig 3 4/C

FIGURE 3. Images from an 86-year-old man diagnosed with pure form dementia with grains (Braak neurofibrillary tangle Stage 2, senile plaque Stage C [mainly diffuse plaques], or Clinical Dementia Rating 3). **(A)** In a cranial magnetic resonance image 4 years before death, there is dilatation of the temporal groove and inferior horn of the lateral ventricle and atrophy of the temporal pole and anterior medial temporal lobe, all with left side dominance. **(B)** A ^{18}F-labeled fluorodeoxyglucose positron emission tomographic image showing hypometabolism of the bilateral anterior medial temporal lobe with left side dominance. **(C)** Fresh coronal section of the right hemisphere showing marked atrophy of the amygdala and ambient gyrus (arrow). Scale = 1 cm. **(D, E)** At the level of the amygdala, there are many argyrophilic grains, with more on the left side **(E)** than on the right side **(D)**. AT8 immunostaining. Bar = 20 μm.

ε4/ε4. All 9 carriers of APOE ε4 showed histopathological asymmetry (statistically not significant vs noncarriers); of these, 1 patient had the pure form, 2 patients had the NFT form, 3 patients had the combined forms (1 patient each with PSP, DLB plus PSP, and CBD), and 3 patients had mixed forms.

DISCUSSION

We demonstrate histopathological asymmetry in the majority (59/65, 90.8%) of the brains examined from patients with AG Stage 3. Because this asymmetry can also be detected by neuroimaging in vivo, its identification may contribute to the clinical diagnosis of DG, particularly in combination with identification of preferential atrophy of the ambient gyrus, a hallmark of DG (10, 11).

The asymmetry in the posterior hippocampus was commensurate with the grain density of the anterior amygdala or the pretangles in the dentate gyrus. Asymmetry in grain density of the anterior amygdala was slightly less frequent than that of the posterior hippocampus, partly because the former seems to be involved in the initial stage of AG disease, and the density may be saturated at a later stage.

We also compared the bilateral maximum density of oligodendroglial coiled bodies in the white matter of parahippocampal gyrus, but there was extensive variability, and we could not perform statistical evaluation. The oligodendroglial coiled bodies observed in various neurodegenerative conditions may not be specific for AG disease.

The rate of detection of cases with histopathological asymmetry was 46.5% in structural neuroimages (CT or MRI) and 100% in functional neuroimages (^{123}I-IMP-SPECT/^{18}F-FDG-PET). The asymmetry in the structural neuroimages of the pure form alone reached 75%. Detection rates might increase if software were developed for voxel-based morphometry based on 3-dimensional MRI, focusing on asymmetry and selective atrophy of the ambient gyrus.

The frequent asymmetry in AG is shared with other tauopathies, including CBD, PSP, and Pick disease with Pick bodies. Patients with AG Stage 3 but without histopathological asymmetry were older and of higher Braak NFT stage than patients with asymmetry. This result may be partly influenced by the difficulty in discriminating AGs and Alzheimer-type neuropil threads in patients with higher Braak NFT stage, even with IHC using a specific antibody raised against the 4-repeat tau isoform (9). Alternatively, it may suggest a pathogenetic relationship between AGs and NFTs.

Argyrophilic grain Stage 3 cases showed asymmetry more often than AD cases by both histopathological and radiological assessments. Asymmetry may also be a feature of hippocampal sclerosis dementia (35), but these cases usually show asymmetry in signal intensity in the hippocampus in FLAIR images or do not show atrophy of the anterior medial temporal lobe, including amygdala (unpublished data).

Apolipoprotein E genotyping of subjects with AG Stage 3 did not demonstrate a correlation between asymmetry and ε2 (36–38). In contrast, although statistically not significant, all 9 ε4 carriers in the patients studied showed histopathological asymmetry. Apolipoprotein E ε4 consists of a risk factor of AD, and this may also be associated with the asymmetry of DG.

This analysis also indicates that patients with left-dominant AG tended to show more severe cognitive decline than patients with right-dominant AG. Among the 65 patients, 41 were right-handed, 1 was left-handed, and the rest did not have handedness recorded. Thus, the language center was most likely located in the left hemisphere in most cases, and it is reasonable to speculate that more extensive damage to the hemisphere dominant for language may result in more severe cognitive decline than involvement of the nondominant hemisphere. Retrospective studies of autopsy-confirmed DG reported that its clinical features are either AD-like amnesia (39–41) or Pick-like frontotemporal dementia (42–45). If clinical diagnosis of DG becomes possible and preferential involvement of either the right or the left hemisphere is determined radiologically, more detailed clinical and pathological correlations could be performed.

Few studies have examined the correlation between radiological and pathological findings of DG. In a postmortem MRI study of the oldest patients (>85 years) with special attention to atrophy of the medial temporal lobe, Barkhof et al (46) reported that 13 (10%) of 132 patients had pure AG disease; 4 of the 13 patients showed significant atrophy involving the medial temporal lobe. Josephs et al (47) used voxel-based morphometry to analyze MRI of AG patients with or without dementia and concluded that the damage visible in the MR image contributed to the clinical manifestation of dementia; however, they did not mention either radiological or pathological asymmetry.

Argyrophilic grains are often associated with other neurodegenerative processes. Because NFT-dominant senile changes are frequently associated with AGs and could modify clinical manifestations, we separated the NFT form from other cases for future analysis. It is notable that all PSP patients with AG Stage 3 showed the commensurate histopathological asymmetry, suggesting that histopathological asymmetry of PSP may be influenced by the histopathological asymmetry of AGs.

In conclusion, left-right asymmetry in density and/or extent of AG is present in most patients with AG Stage 3 and is detectable by antemortem morphological and functional neuroimaging. In combination with the finding of preferential atrophy of the ambient gyrus, detection of this asymmetry could contribute to the clinical diagnosis of DG.

ACKNOWLEDGMENTS

The authors thank Mr Naoo Aikyo, Mr Fumio Hasegawa, Ms Mieko Harada, Ms Yuki Kimura, and Ms Nobuko Naoi for the preparation of sections and Dr Kinuko Suzuki for helpful discussions. The authors also thank 2 anonymous neurologists for preparing the CDR ratings used in this study.

REFERENCES

1. Braak H, Braak E. Argyrophilic grains: Characteristic pathology of cerebral cortex in cases of adult onset dementia without Alzheimer changes. Neurosci Lett 1987;76:124–27

2. Braak H, Braak E. Argyrophilic grain disease: Frequency of occurrence in different age categories and neuropathological diagnostic criteria. J Neural Transm 1998;105:801–19
3. Jellinger KA. Dementia with grains (argyrophilic grain disease). Brain Pathol 1998;8:377–86
4. Tolnay M, Clavaguera F. Argyrophilic grain disease: A late-onset dementia with distinctive features among tauopathies. Neuropathology 2004;24:269–83
5. Ikeda K, Akiyama H, Kondo H, et al. A study of dementia with argyrophilic grains. Possible cytoskeletal abnormality in dendrospinal portion of neurons and oligodendroglia. Acta Neuropathol 1995;89:409–14
6. Togo T, Sahara N, Yen SH, et al. Argyrophilic grain disease is a sporadic 4-repeat tauopathy. J Neuropathol Exp Neurol 2002;61:547–56
7. Tolnay M, Sergeant N, Ghestem A, et al. Argyrophilic grain disease and Alzheimer's disease are distinguished by their different distribution of tau protein isoforms. Acta Neuropathol 2002;104:425–34
8. Zhukareva V, Shah K, Uryu K, et al. Biochemical analysis of tau proteins in argyrophilic grain disease, Alzheimer's disease, and Pick's disease: A comparative study. Am J Pathol 2002;161:1135–41
9. Fujino Y, Wang DS, Thomas N, et al. Increased frequency of argyrophilic grain disease in Alzheimer disease with 4*R* tau-specific immunohistochemistry. J Neuropathol Exp Neurol 2005;64:209–14
10. Saito Y, Yamazaki M, Kanazawa I, et al. Severe involvement of the ambient gyrus in a case of dementia with argyrophilic grain disease. J Neurol Sci 2002;196:71–75
11. Saito Y, Nakahara K, Yamanouchi H, et al. Severe involvement of ambient gyrus in dementia with grains. J Neuropathol Exp Neurol 2002; 61:789–96
12. Saito Y, Ruberu NN, Sawabe M, et al. Staging of argyrophilic grains: An age-associated tauopathy. J Neuropathol Exp Neurol 2004;63:911–18
13. Ferrer I, Santpere G, van Leeuwen FW. Argyrophilic grain disease. Brain 2008;131:1416–32
14. Santpere G, Ferrer I. Delineation of early changes in cases with progressive supranuclear palsy-like pathology. Astrocytes in striatum are primary targets of tau phosphorylation and GFAP oxidation. Brain Pathol 2009;19:177–87
15. Fumimura Y, Ikemura M, Saito Y, et al. Analysis of the adrenal gland is useful for evaluating pathology of the peripheral autonomic nervous system in Lewy body disease. J Neuropathol Exp Neurol 2007;66: 354–62
16. Yamaguchi H, Haga C, Hirai S, et al. Distinctive, rapid, and easy labeling of diffuse plaques in the Alzheimer brains by a new methenamine silver stain. Acta Neuropathol 1990;79:569–72
17. Gallyas F. Silver staining of Alzheimer's neurofibrillary changes by means of physical development. Acta Morphol Acad Sci Hung 1971; 19:1–8
18. Saito Y, Kawashima A, Ruberu NN, et al. Accumulation of phosphorylated alpha-synuclein in aging human brain. J Neuropathol Exp Neurol 2003;62:644–54
19. Wenham PR, Price WH, Blandell G. Apolipoprotein E genotyping by one-stage PCR. Lancet 1991;337:1158–59
20. Hixson JE, Vernier DT. Restriction isotyping of human apolipoprotein E by gene amplification and cleavage with *Hha*I. J Lipid Res 1990;31: 545–48
21. Kuwano R, Miyashita A, Arai H, et al. Dynamin-binding protein gene on chromosome 10q is associated with late-onset Alzheimer's disease. Hum Mol Genet 2006;15:2170–82
22. Folstein MF, Folstein SE, McHugh PR. "Mini-Mental State." A practical method for grading the cognitive state of patients for the clinician. J Psychiatr Res 1975;12:189–98

AQ2 23. Hasegawa KI IK, Moriya K. An investigation of dementia rating scale for the elderly. Seishin Igaku 1974;16:965–69

24. Lawton MP, Brody EM. Assessment of older people: Self-maintaining and instrumental activities of daily living. Gerontologist 1969;9:179–86
25. Hughes CP, Berg L, Danziger WL, et al. A new clinical scale for the staging of dementia. Br J Psychiatry 1982;140:566–72
26. Braak H, Braak E. Neuropathological stageing of Alzheimer-related changes. Acta Neuropathol 1991;82:239–59
27. Murayama S, Saito Y. Neuropathological diagnostic criteria for Alzheimer's disease. Neuropathology 2004;24:254–60
28. Jellinger KA, Bancher C. Senile dementia with tangles (tangle predominant form of senile dementia). Brain Pathol 1998;8:367–76
29. McKeith IG, Dickson DW, Lowe J, et al. Diagnosis and management of dementia with Lewy bodies: Third report of the DLB Consortium. Neurology 2005;65:1863–72
30. Hauw JJ, Daniel SE, Dickson D, et al. Preliminary NINDS neuropathologic criteria for Steele-Richardson-Olszewski syndrome (progressive supranuclear palsy). Neurology 1994;44:2015–19
31. Dickson DW, Bergeron C, Chin SS, et al. Office of Rare Diseases neuropathologic criteria for corticobasal degeneration. J Neuropathol Exp Neurol 2002;61:935–46
32. Roman GC, Tatemichi TK, Erkinjuntti T, et al. Vascular dementia: Diagnostic criteria for research studies. Report of the NINDS-AIREN International Workshop. Neurology 1993;43:250–60
33. Saito Y, Ruberu NN, Sawabe M, et al. Lewy body–related alpha-synucleinopathy in aging. J Neuropathol Exp Neurol 2004;63:742–49
34. Alafuzoff I, Arzberger T, Al-Sarraj S, et al. Staging of neurofibrillary pathology in Alzheimer's disease: A study of the BrainNet Europe Consortium. Brain Pathol 2008;18:484–96
35. Probst A, Taylor KI, Tolnay M. Hippocampal sclerosis dementia: A reappraisal. Acta Neuropathol 2007;114:335–45
36. Ghebremedhin E, Schultz C, Botez G, et al. Argyrophilic grain disease is associated with apolipoprotein E epsilon 2 allele. Acta Neuropathol 1998; 96:222–24
37. Togo T, Cookson N, Dickson DW. Argyrophilic grain disease: Neuropathology, frequency in a dementia brain bank and lack of relationship with apolipoprotein E. Brain Pathol 2002;12:45–52
38. Tolnay M, Probst A, Monsch AU, et al. Apolipoprotein E allele frequencies in argyrophilic grain disease. Acta Neuropathol 1998;96: 225–27
39. Saito Y, Murayama S. Neuropathology of mild cognitive impairment. Neuropathology 2007;27:578–84
40. Petersen RC, Parisi JE, Dickson DW, et al. Neuropathologic features of amnestic mild cognitive impairment. Arch Neurol 2006;63:665–72
41. Jicha GA, Petersen RC, Knopman DS, et al. Argyrophilic grain disease in demented subjects presenting initially with amnestic mild cognitive impairment. J Neuropathol Exp Neurol 2006;65:602–9
42. Steuerwald GM, Baumann TP, Taylor KI, et al. Clinical characteristics of dementia associated with argyrophilic grain disease. Dement Geriatr Cogn Disord 2007;24:229–34
43. Togo T, Isojima D, Akatsu H, et al. Clinical features of argyrophilic grain disease: A retrospective survey of cases with neuropsychiatric symptoms. Am J Geriatr Psychiatry 2005;13:1083–91
44. Ikeda K, Akiyama H, Arai T, et al. Clinical aspects of argyrophilic grain disease. Clin Neuropathol 2000;19:278–84
45. Ishihara K, Araki S, Ihori N, et al. Argyrophilic grain disease presenting with frontotemporal dementia: A neuropsychological and pathological study of an autopsied case with presenile onset. Neuropathology 2005;25: 165–70
46. Barkhof F, Polvikoski TM, van Straaten EC, et al. The significance of medial temporal lobe atrophy: A postmortem MRI study in the very old. Neurology 2007;69:1521–27
47. Josephs KA, Whitwell JL, Parisi JE, et al. Argyrophilic grains: A distinct disease or an additive pathology? Neurobiol Aging 2008;29:566–73